How the distribution of relaxation times enhances complex equivalent circuit models for fuel cells

Sebastian Dierickx*, André Weber, Ellen Ivers-Tiffée

Institute for Applied Materials (IAM-WET), Karlsruhe Institute of Technology (KIT), Adenauerring 20b, 76131 Karlsruhe, Germany

ARTICLE INFO

Keywords:
Electrochemical impedance spectroscopy
Distribution of relaxation times
SOFC
PEMFC
Equivalent circuit modelling

ABSTRACT

Distribution of relaxation times (DRT) is a well-established method for deconvoluting electrochemical impedance spectroscopy (EIS) data from fuel cells. DRT-analysis provides a deeper insight into electrode reactions and supports identification of the most accurate equivalent circuit models. This established method has undergone much change in recent decades and has been applied to many sub-fields. Contemporary studies are highly specialized and produce specialist literature: to further a comprehensive view, this paper provides an overview and retrospective. EIS measurement and subsequent interpretation by DRT are challenging because (i) high-performance electrodes have very low impedances (10–100 mΩ), (ii) the concept of one rate-limiting step is usually not applicable, and (iii) the charge transfer and transport processes in anode and cathode are often coupled; overlapping in the frequency domain. In this paper selected results from advanced EIS and DRT analyses are discussed. We demonstrate the importance of EIS data quality, introduce the use of the Kramers-Kronig transformation, explain the impacts of statistically distributed noise and single errors in EIS spectra, and the selection of the regularization parameter lambda for improved interpretation of DRT curves. Finally, well-selected examples of DRT approaches lead to adequate models with different complexity. As a result, this paper deepens the understanding of how to assess electrochemical measurements of fuel cells based on the DRT. It, therefore, represents a vital guide for DRT analysis.

Glossary

2CTLM	Two-channeled Transmission Line Model (1 layer)
3CTLM	Three-channeled Transmission Line Model (2 layers)
AC	Alternating Current
AFL	Anode Functional Layer
AS	Anode Substrate
ASC	Anode Supported Cell
AWGN	Additive White Gaussian Noise
CNLS	Complex Non Linear Square
DC	Direct Current
DRT	Distribution of Relaxation Times
ECM	Equivalent Circuit Model
EIS	Electrochemical Impedance Spectroscopy
FIB	Focused Ion Beam
GFLW	Generalized Finite-Length Warburg Element
KK	Kramers-Kronig
LSCF	$La_{0.58}Sr_{0.4}Co_{0.2}Fe_{0.8}O_{3-\delta}$
MCFC	Molten Carbonate Fuel Cell
PCFC	Protonic Ceramic Fuel Cell
PEMFC	Polymer Electrolyte Fuel Cell
OCC	Open Circuit Condition
OCV	Open Circuit Voltage
SEM	Scanning Electron Microscope
SOFC	Solid Oxide Fuel Cell
TPB	Triple Phase Boundary
TLM	Transmission Line Model
YSZ	Yttrium (III) Oxide (Y_2O_3) stabilized Zirconia: $Y_{0.16}Zr_{0.84}O_{2-\delta}$

1. Introduction

1.1. Electrochemical Impedance Spectroscopy (EIS)

Electrochemical impedance spectroscopy (EIS) and the related frequency response analysis are well-established methods for investigating electrochemical devices and components. Already in the 19th century initial investigations on frequency-dependent material characteristics, mainly for dielectrics and ferroelectrics, were performed. Todayś common approach of determining the electrolyte resistance and conductivity by AC-measurements and thus eliminating electrode polarizations was already introduced in 1869

* Corresponding author.
E-mail address: sebastian.dierickx@kit.edu (S. Dierickx).

[1] and the related challenges were summarized in [2]. Since then, the theoretical background of equivalent circuit models [3] has evolved, as well as the analysis of materials by AC-methods, commonly displayed in Cole-Cole plots [4]. Bauerle investigated polarization in solid zirconia electrolytes [5], and first proved the usefulness of AC-measurements for polycrystalline solids when applied in fuel cells. The availability of commercial frequency response analyzer equipment as well as well-suited software for analyzing impedance data [6,7] broadened the research work dramatically.

Historical aspects of impedance spectroscopy are summarized in [8], while the theory is comprehensibly presented in the books of Macdonald [8], Orazem [9] and Lasia [10]. EIS spectra should be free of any type of error, either arising from the measurement equipment or the instability of the sample under test [11]. We recommend proving the validity of measured spectra first, i.e., by algorithms based on the Kramers-Kronig relation [12,13]. Appropriate software tools are available, e.g. free of charge on our group's website [14]. However, the interpretation of measured impedances still poses a major challenge today. To cope with this difficulty the application of the Distribution of Relaxation Times (DRT) propagates itself more and more as an invincible evaluation method for resolving impedance data.

1.2. Distribution of Relaxation Times (DRT)

The correct calculation and suitable application of the DRT require extensive basic knowledge, which we want to impart in the scope of this publication. In this regard, we summarize retrospectively the supportive findings of previous DRT-related publications on fuel cells. This is, in our view, of fundamental importance for the realization of a vital guideline covering all important features of the DRT analysis.

More than a century ago, Schweidler introduced the idea of distributed relaxation times in [15], which was further promoted by Wagner [16]. Since then, only a few publications featuring a Distribution of Relaxation Times (DRT) [4,17] and unfolding of EIS spectra by a DRT were available before the year 2000 [18–24]. These mostly considered dielectric materials. Schichlein [25] published in 2002 a methodology for calculating the DRT from the EIS spectra of a single, planar solid oxide fuel cell (SOFC). He showed that the DRT method deconvolutes processes with rather close time constants in porous SOFC electrodes, and thereby provided a clearer insight into electrochemical reactions and transport.

The relation between the impedance spectrum $Z(\omega)$ and the DRT $\gamma(\tau)$ - mostly displayed as $g(f)$, e.g. distribution of the relaxation frequencies - is given by:

$$Z(\omega) = R_0 + Z_{\mathrm{Pol}}(\omega) = R_0 + \int_0^\infty \frac{\gamma(\tau)}{1 + \mathrm{j}\omega\tau}\mathrm{d}\tau. \qquad (1)$$

This relation is valid for any valid impedance spectrum that fulfills linearity, causality and time invariance criteria. Even though this equation looks "capacitive", i.e., an infinite number of RC-elements connected in series, it is not limited to capacitive processes as derived by Schönleber in [29]. The applicability of an extended DRT considering pseudo-inductive processes in PEMFC impedance spectra is shown in [27].

The calculation of the DRT is not straight forward as the required inversion of Eq. (1), is an ill-posed problem (Fredholm integral [28]). One approach is based on a discrete Fourier transformation applied to the imaginary part of $Z(\omega)$ [25]. The indispensable data extrapolation and filtering is challenging and extremely high demands concerning impedance data quality have to be fulfilled [29]. To overcome these problems a few years later Sonn [30] applied a fitting approach (fitting the real part of the spectra to a number of RC-elements with fixed time constants) combined with the Tikhonov regularization. The related Ftikreg source code is available at [31], and further details are published by Weese [32]. Alternatively, the Tikhonov regularization–based DRT can be calculated simultaneously with the freely available software DRTTools programmed by the Ciucci group [33,34]. The DRT calculation herewith incorporates several input values: the represented frequency range of the DRT, the number of points per decade, the number of impedance values considered in the calculation and the regularization parameter, λ. Those values are based on a judgment of the residuals for the DRT calculation (as demonstrated in the next section for varying λ) as well as on the user's experience. The most valuable importance, however, stems from the regularization parameter λ, which smoothens the DRT and avoids artificial peaks. To our group's experience, it is crucial to identify the best-suited value of the regularization parameter for each set of impedance data. Once identified, using the *same* value of the regularization parameter for all impedance curves within this set it is of utmost importance. For the sake of completeness, meaningful details are found in Boukamp's work [35,36], who describes and compares Tikhonov regularization as well as the DRT calculation via Fourier transformation and multiple (RQ)-method.

In the past ten years, the DRT became appealing for even more researchers, who presented several tools for calculating the DRT and applying it to the impedance analysis of fuel cells [37–45].

Common ways to display impedance spectra are Nyquist- or Bode-plots, which unfortunately prevent the identification of individual processes with close relaxation frequencies or time constants. Fig. 1 shows the impedance spectrum for two RC-elements, each consisting of a resistance, R, in parallel to a capacitor, C, with the time constants $\tau_2 = 2 \cdot \tau_1$ ($\tau_i = R_i C_i = 1/(2\pi f_i)$). The existence of two individual RC-elements is neither discernible in the Nyquist plot (cf. Fig. 1 (a)) nor in the Bode plot (cf. Fig. 1 (b)). On the contrary, two Dirac-pulses result from the analytically calculated DRT [17] (cf. Fig. 1 (c)), and are exactly located at their relaxation frequency. But this analytical calculation is not applicable for discrete impedance values. Thus, numerical methods are indispensable (please see [25] and [30]). In this publication, the DRT was calculated using the software package Ftikreg [32] from the (generally less noisy) real part of the impedance spectrum $Z(\omega)$, as shown in Fig. 1 (d). Both numerical and analytical DRT resolve the two processes. The heights and widths of the peaks differ slightly, even though they should be very similar; but this is related to numerical issues in the DRT calculation.

The following sections will explain both the analytical and the numerical DRT of common equivalent circuit elements. In this context, it is important to us to present and discuss essential properties and possibilities of the DRT analysis – such as the influence of regularization on the DRT and the measurement data quality of SOFC and PEMFC impedances before applying the DRT to develop equivalent circuit models. For a better understanding of these new contexts, a suitable framework that encompasses the theory of DRT is deemed necessary. Parts of it were already published in our previous publication [46], but are now widely expanded by, i.e., new graphs and simulations as well as a stepwise deduction of ECM models of increasing complexity.

2. DRT Calculation

2.1. Analytical and numerical DRT of common equivalent circuit elements

When considering the impedance spectra of fuel cells, a number of common equivalent circuit elements (e.g. RQ-, Gerischer- and Warburg-elements) can enable a physically meaningful representation of transport and reaction processes in multiphase gas diffusion electrodes [47]. The impedance of these elements is given in an analytical form and it is possible to calculate the analytical DRT

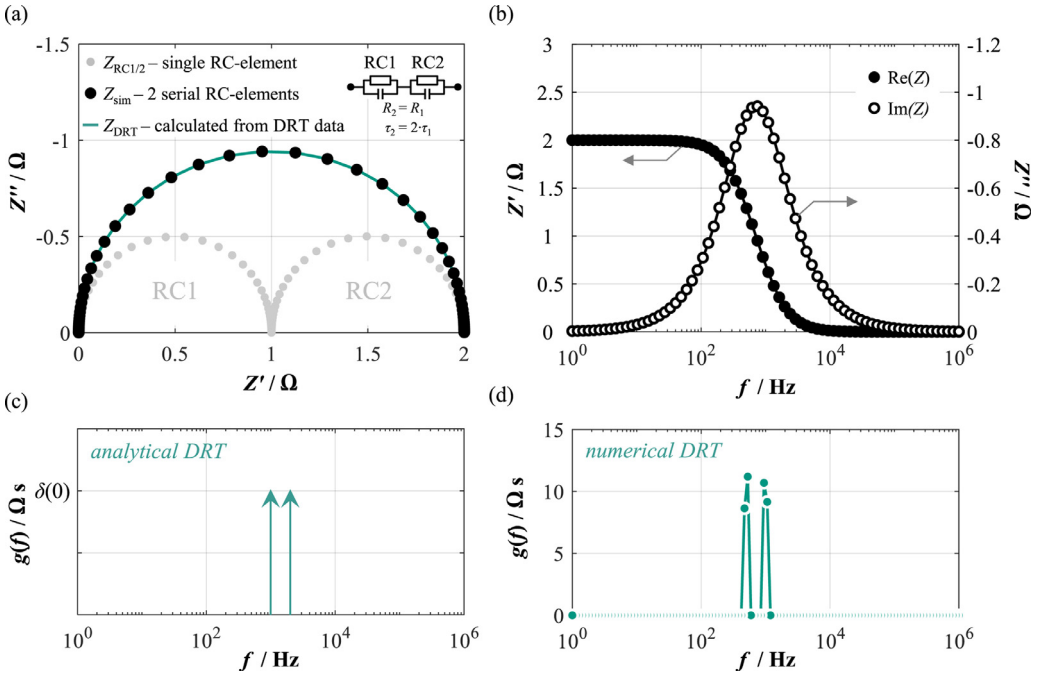

Fig. 1. An impedance spectrum of two serial RC-elements with the time constants $\tau_2 = 2 \cdot \tau_1$ and $R_2 = R_1$ displayed as (a) Nyquist plot, (b) real and imaginary part vs. frequency, (c) analytical and (d) numerical DRT.

based on the impedance term. The following section presents the analytical DRTs of these common equivalent circuit elements and compares them with appropriate numerical DRTs calculated from simulated impedance spectra. A fully detailed account of the analytical DRT calculation of common equivalent circuit elements is reported, i.e., by Leonide in [48] and by Boukamp in [49].

RQ-element - An RQ-element (parallel connection of resistance R and constant phase element Q):

$$Z_{RQ}(\omega) = \frac{R}{1 + R \cdot Q^{-1}}, \tag{2}$$

with the constant phase element Q:

$$Z_Q(\omega) = Q(\omega) = \frac{1}{(j\omega)^{n_Q} \cdot Y_Q}, \text{with } 0 \le n_Q \le 1. \tag{3}$$

exhibits the analytical DRT as given in Eq. (4) (with $x = \ln(\omega)$) [48,50]:

$$g_{RQ}(x) = \frac{R_{Pol}}{2 \cdot \pi} \cdot \frac{\sin((1 - n_Q) \cdot \pi)}{\cosh(n_Q \cdot (x + \ln(\tau_{RQ}))) - \cos((1 - n_Q) \cdot \pi)}. \tag{4}$$

Fig. 2 (a) shows the DRTs of RQ-elements differing in their n_Q-value. From $n_Q = 1$ (ideal RC-element) the height of the peak decreases and its width increases with decreasing n_Q. In comparison to the analytical DRT, the peak of the numerical DRT is more spread within the frequency domain and has additional, small, symmetrically-arranged peaks, which result from the finite frequency range.

GFLW-element - The highly asymmetric finite-length Warburg-element:

$$Z_{GFLW}(\omega) = R_W \cdot \frac{\tanh\left((j\omega\tau_W)^{n_W}\right)}{(j\omega\tau_W)^{n_W}}, \text{ with } 0 \le n_W \le 0.5, \tag{5}$$

exhibits a rather complex analytical DRT (with $x = \ln(\omega)$) [48] (a comparable expression was derived from [49]):

$$g_{GFLW}(x) = -\frac{R_W}{\pi} \cdot \left(\begin{array}{l} \frac{1}{2} e^{-\frac{(j\pi + 2x) \cdot n_W}{2}} \cdot \frac{1}{{\tau_W}^{n_W}} \cdot \operatorname{sech}\left((e^x \tau_W)^{n_W}\right) \\ \cdot \operatorname{sech}\left(\left(e^{j\pi + x} \tau_W\right)^{n_W}\right) \\ \left[\begin{array}{l} \cos\left(\frac{\pi \cdot n_W}{2}\right) \cdot \sin\left(2 \cdot (j e^x \tau_W)^{n_W} \cdot \sin\left(\frac{\pi \cdot n_W}{2}\right)\right) \\ -\sin\left(\frac{\pi \cdot n_W}{2}\right) \cdot \sinh\left(2 \cdot (j e^x \tau_W)^{n_W} \cdot \cos\left(\frac{\pi \cdot n_W}{2}\right)\right) \end{array} \right] \\ -\frac{1}{2} j \frac{1}{(e^x \tau_W)^{n_W}} \cdot \left(\begin{array}{l} \tanh\left((e^x \tau_W)^{n_W}\right) \\ -e^{j\pi \cdot n_W} \cdot \tanh\left(\left(e^{-j\pi + x} \cdot \tau_W\right)^{n_W}\right) \end{array} \right) \end{array} \right). \tag{6}$$

It is of importance, that the dominant peak at the characteristic frequency is escorted by smaller peaks at higher frequencies. Warburg- and Gerischer-element (introduced below) represent asymmetric equivalent circuit elements, and their corresponding DRT curve will broaden over several decades of frequency. This feature complicates the identification of individual minor processes within the same frequency range. In this case, our group selects appropriate experimental parameters (i.e., new gas compositions [51]) and shifts the relevant relaxation frequencies thereby. Alternatively, Boukamp showed that by applying the multiple (RQ)-method to calculate the DRT, the side peaks are then less regularized and can be better resolved (but tend to be overestimated) [52]. Nevertheless, it is essential to perform the above-mentioned experiments to act against possible overlapping in the frequency domain. Due to the regularization, the number of peaks in the numerical DRT is considerably lower (cf. Fig. 2 (b)).

Gerischer-element - A similar behavior to that of the GFLW is observed for the Gerischer-element:

$$Z_G(\omega) = \frac{R_G}{\sqrt{1 + j\omega\tau_G}}, \tag{7}$$

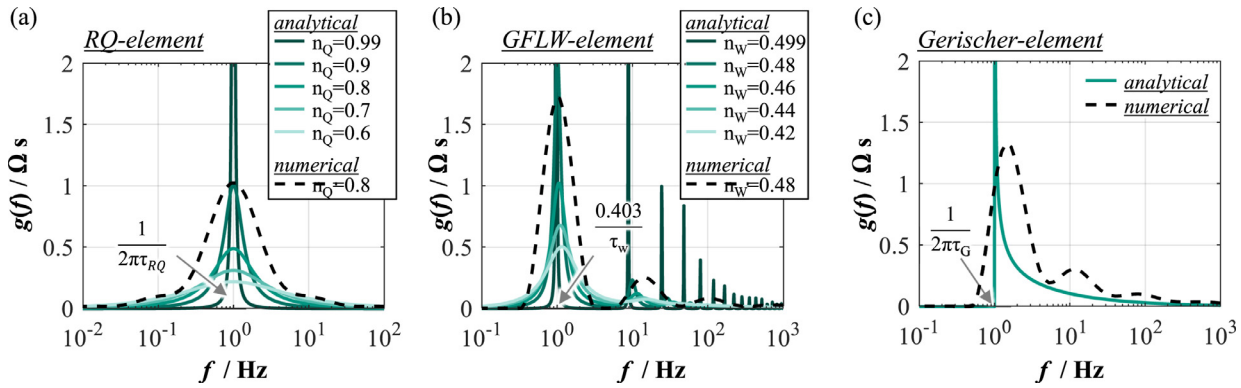

Fig. 2. Analytical DRT of (a) an RQ-element according to Eq. (4) with different n_Q-values, (b) of a finite-length Warburg-element according to Eq. (6) with different n_W-values with different n_Q-values and (c) of a Gerischer-element according to Eq. (8). In addition the numerical DRT of all elements calculated with $\lambda = 10^{-2}$ is shown for selected n-values. All simulations are based on $R_i = 1\ \Omega$ and $f_i = 1$ Hz.

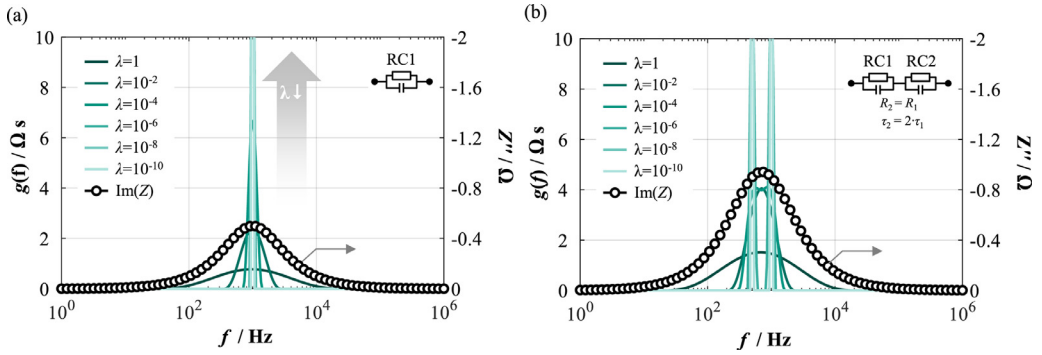

Fig. 3. DRTs of (a) an RC-element and (b) a spectrum consisting of two RC-elements (with $\tau_2 = 2 \cdot \tau_1$ and $R_2 = R_1$), calculated by the Tikhonov regularization using different λ-values.

with the corresponding DRT (with $x = \ln(\omega)$), a complex-valued function with a singularity at $x = \ln(1/\tau_G)$:

$$g_G(x) = \frac{\sqrt{2}\cdot R_G}{\pi} \cdot \sqrt{\frac{\sqrt{1-(e^x\cdot\tau_G)^2}-1}{1-(e^x\cdot\tau_G)^2}}, \tag{8}$$

which can be simplified [48] to:

$$g_G(x) = \begin{cases} \mathrm{Re}\left\{\dfrac{\sqrt{2}\cdot R_G}{\pi}\cdot\sqrt{\dfrac{\sqrt{1-(e^x\cdot\tau_G)^2}-1}{1-(e^x\cdot\tau_G)^2}}\right\} & \text{for } x \geq \ln\left(\dfrac{1}{\tau_G}\right), \\ 0 & \text{for } x < \ln\left(\dfrac{1}{\tau_G}\right). \end{cases} \tag{9}$$

Fig. 2 (c) displays the analytical and numerical DRT of a Gerischer-element. The curvatures differ markedly, as also demonstrated by Boukamp [49].

3. Numerical DRT calculation by Tikhonov regularization

The Tikhonov regularization is primarily controlled by one important parameter; the regularization parameter, λ, which weights the regularization and thus determines the smoothness of the DRT. For numerical DRTs, Eq. (1) is reduced to the sum of a finite number of RC-elements per decade [53]. Fig. 3 (a) exemplifies the effect of λ on the DRT for an RC-element. Decreasing the parameter λ changes the DRT peak in width and height, and increases the DRT resolution.

This effect is also visible in Fig. 3 (b) for the case of two serial RC-elements (with $\tau_2 = 2 \cdot \tau_1$ and $R_2 = R_1$), which are clearly resolvable for λ-values $\leq 10^{-8}$, whereas the imaginary part vs. frequency only resolves one process.

3.1. Robustness of the DRT in regard to the data quality

Down to here, all DRT examples were calculated from synthetic impedance data. Thus, this kind of spectra represents discrete values within a limited frequency range and resolution. In the contrary, measured spectra always interfere with measurement errors or noise arising from the test equipment or the sample under test itself [11]. Fig. 4 (a) shows an impedance spectrum of three serial RC-elements with spread time constants ($\tau_2 = 10 \cdot \tau_1$ and $R_2 = R_2$), overlaid with and without statistically distributed noise (20 dB additive white gaussian noise (AWGN). The synthetic spectrum resembles a simplified impedance of a fuel cell by one series resistance and three serial RC-elements.

Regardless of whether with or without AWGN, both DRT curves appear rather similar. The statistically distributed errors are compensated by the regularization. Additional peaks caused by noisy data points cannot be fully avoided.

However, noise compensation reaches its limits with narrow time constants. Fig. 4 (b) displays the DRT of three serial connected RC-elements; the relaxation frequencies of the first two RC-elements are very narrow ($\tau_2 = 2 \cdot \tau_1$), similar to Fig. 3 (b). In this example, the noise prevents the resolution of the two high-frequency peaks. Besides, randomly distributed artificial peaks appear in the DRT at high frequencies.

While regularization can to some extent handle the before mentioned statistically distributed noise, occasionally erroneous data points falsify the DRT calculation. As shown in Fig. 5 (a&b), a single erroneous data point at 50 Hz already leads to a significant deviation in peak size and frequency. Thereby the impact is most severe if the data error interferes with the surrounding peaks. The contrary scenario is demonstrated in Fig. 5 (c&d). Here, the distortion is less observable, because the distance of the middle peak to

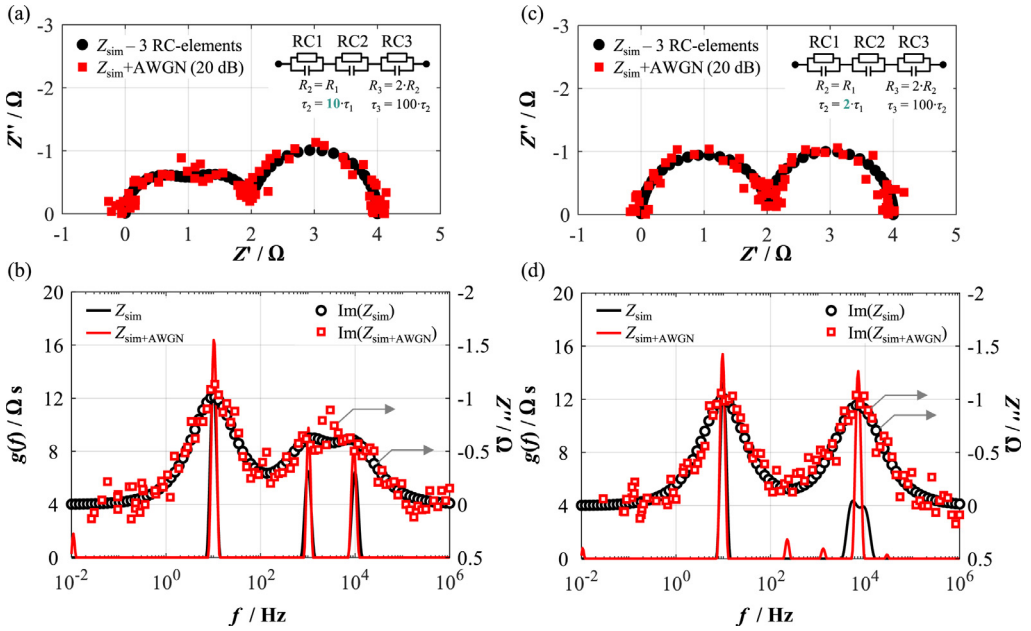

Fig. 4. (a) Impedance spectrum of three serial RC-elements with spread time constants ($\tau_2 = 10 \cdot \tau_1$ and $R_2 = R_2$), overlaid with and without Noise (20 dB AWGN). (b) Imaginary part of the impedance spectra in (a) and the calculated DRTs ($\lambda = 10^{-4}$). Here (c) and (d) show the corresponding impedance spectra and DRTs for narrow time constants ($\tau_2 = 2 \cdot \tau_1$).

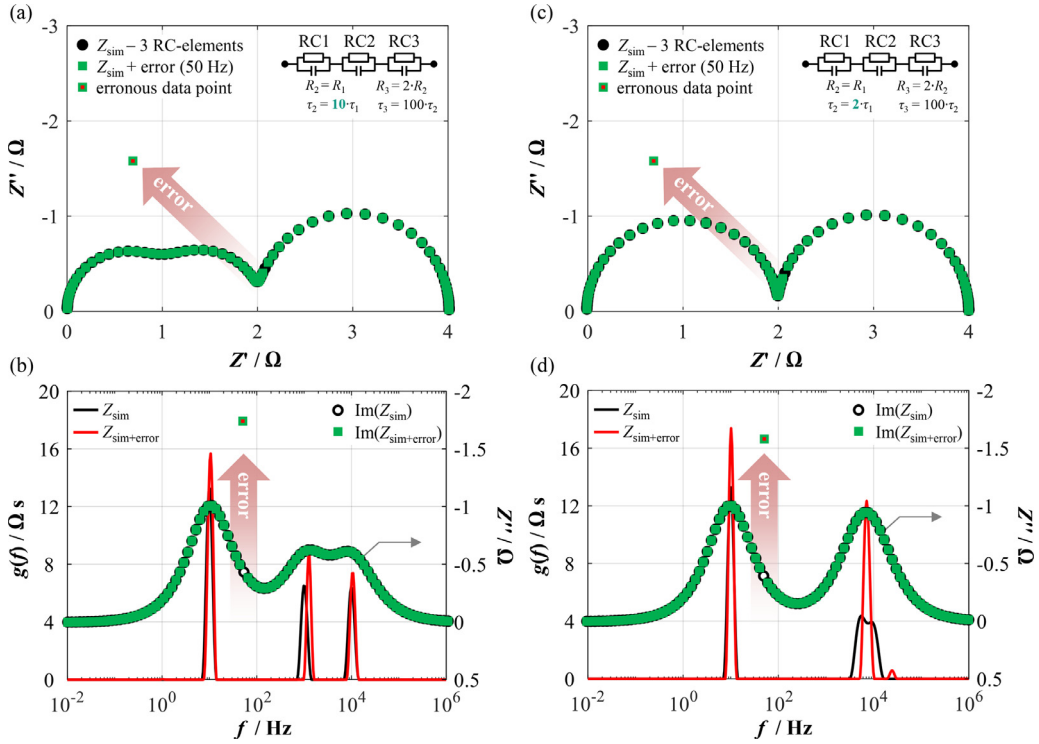

Fig. 5. (a) Impedance spectrum and (b) DRT of three serial RC-elements with spread time constants ($\tau_2 = 10 \cdot \tau_1$) and one erroneous data point at 50 Hz ($\lambda = 10^{-4}$). Removing this data point from the spectrum removes the errors in the DRT. Here (c) and (d) show the corresponding impedance spectra and DRTs for narrow time constants ($\tau_2 = 2 \cdot \tau_1$).

the faulty data point is larger. For a sound DRT calculation, however, such errors must be removed first.

The previous examples verify, that high quality measured impedance spectra are indispensable for trustworthy DRT results.

In the same way, the quality of the impedance spectrum determines the best possible choice of the λ-value. Generally speaking, the λ should be selected to be (i) as small as possible to obtain a good resolution and (ii) as large as needed to suppress artifacts. This distinction is made after repeated experiments with varying operating conditions. Parts of the DRT show physically meaningful behavior while others just randomly vary. Automatic procedures may give a false sense of security to the user (see next section). Hanke, who examined the problem of regularization techniques from a mathematician's point of view, stated that "*No black-box procedures for choosing the regularization parameter λ are available, and most likely will never exist*" [54].

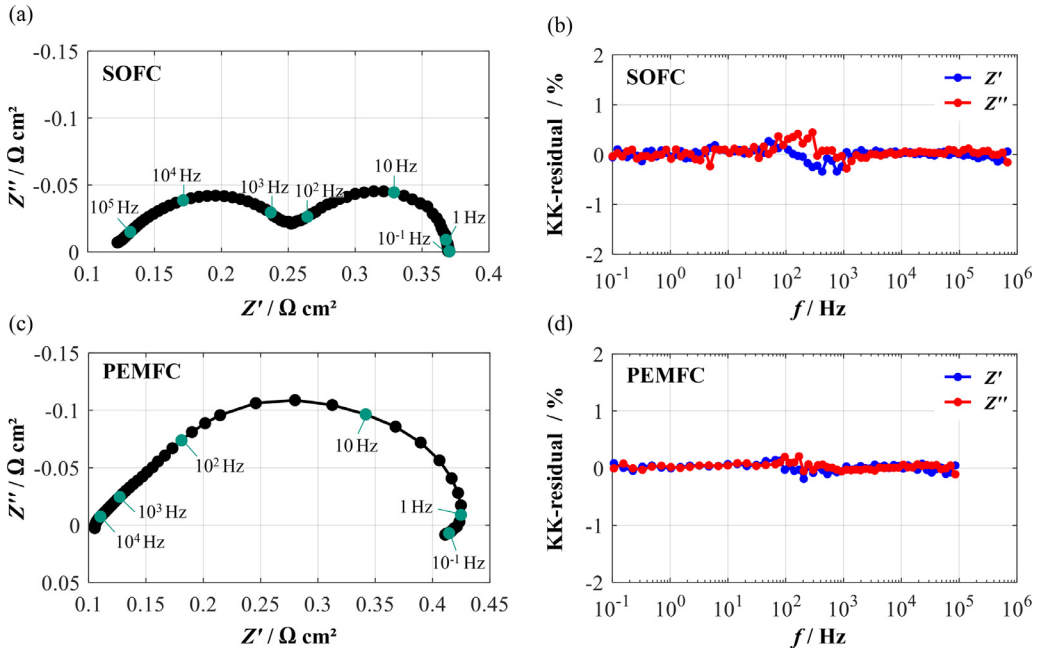

Fig. 6. Valid impedance spectra of (a) an anode-supported SOFC recorded under OCV-conditions at 720 °C, with 20 % humidified hydrogen as fuel and ambient air as oxidant and (c) a PEMFC recorded at 382 mA cm^{-2}, 80 °C, with humidified hydrogen as fuel (70 % relative humidity) and humidified ambient air as oxidant (70 % relative humidity). Here (b) and (d) show the Kramers-Kronig-residuals of the real (Z') and imaginary part (Z'') of the impedances. (SOFC data from [56]; PEMFC data from [57]).

4. DRT analysis of fuel cell impedance spectra

4.1. Impedance data quality and regularization parameter

As demonstrated in the previous section, data quality is crucial for reliable impedance spectra interpretation. The quality and quantity of the extractable information are implicitly connected to the noise-level and the compliance of the measured spectra with the principles of causality, linearity and stability. When these conditions are fulfilled, the DRT calculation from the impedance data is meaningful. The Kramers-Kronig test is a powerful and independent test for the validity of an impedance spectrum [12,13,55] which meets the required criteria based on the Kramers-Kronig relations. Quick and automated testing of data quality can be performed with the free tool given in [14]. A detailed study on how to interpret the resulting KK-residuals and how they are influenced by measurement parameters and errors is given in [11]. Furthermore, [11] provides key rules for setting up reliable EIS measurements on fuel cells.

As an example of a high-quality impedance spectrum of a solid oxide fuel cell (SOFC) and a proton exchange membrane fuel cell (PEMFC), Fig. 6 (a&c) depict valid impedance spectra. The corresponding KK-residuals are shown in Fig. 6 (b&d) and are below 0.5 % over the whole measured frequency range (SOFC: 1 mHz – 700 kHz; PEMFC: 1 mHz – 90 kHz). It should be pointed out that the displayed spectra have neither been smoothened nor corrected to remove inductive artifacts at high frequencies. It should also be noted that the high impedance data quality requires appropriate test setups and operating conditions. Indispensable measures include DC-furnaces, humidification of gases in catalytic burners, avoidance of liquid water in gas lines and flowfields, as well as appropriate electrical connection and wiring. Whereas SOFCs can be characterized at open circuit voltage (OCV), in the case of PEMFCs any surface oxidation of the platinum catalyst will falsify the results at OCV. Thus, PEMFC impedance spectra should always be measured at sufficiently high current densities.

Besides the quality of the raw impedance data, the interpretability of the DRT highly depends on the correct regularization within the calculation procedure. However, the choice of the optimal regularization parameter λ, is not a trivial issue. As illustrated in Fig. 3 for one and two RC-elements, the chosen λ defines (i) the shape and (ii) the number of deconvolutable peaks. When applying the DRT to measured impedance spectra the choice of the optimal λ becomes even more critical, since the diverse internal processes overlap in the frequency domain. In recent years, several mathematical approaches have been proposed to automatically determine the optimal λ for Tikhonov regularization (not only for the field of fuel cells), these include - the discrepancy method [58], generalized cross-validation technique [59], normalized cumulative periodogram method [60] and most recently the L-curve criterion [61]. In our opinion, however, such procedures should be treated with caution, as we will explain in the following.

Fig. 7 shows an example of the effect of different λ-values for the measured impedance spectrum in Fig. 6 (a). In general, a high λ provides a smooth solution with fewer peaks (and thus less information), whereas a small λ leads to over-interpretation of the data. Therefore, λ should be chosen to be (i) as small as possible to ensure a good resolution of the processes and (ii) as large as necessary to avoid false peaks in the DRT spectrum. A useful criterion for finding the optimal λ is achieved by retransforming the regularized DRT to an impedance for different λ-values, and then comparing the retransformed impedance (Z_{DRT}) with the originally measured impedance (Z_{meas}). An absolute or systematic deviation between the real parts of the impedance spectra (cf. Fig. 7) can serve as an indicator for insufficiently regularized DRTs, and thus defines the upper limit of λ. For the given example, regularization with $\lambda \leq 10^{-2}$ yields an excellent accordance, whereas further reduction of λ has no effect on the deviation. However, as already mentioned, a purely mathematical restriction of lambda towards smaller values is not meaningful, since a distinction between measurement artifacts and physical processes can only be achieved through extensive parameter studies and a comprehensive physical understanding. At this point, we would like to once

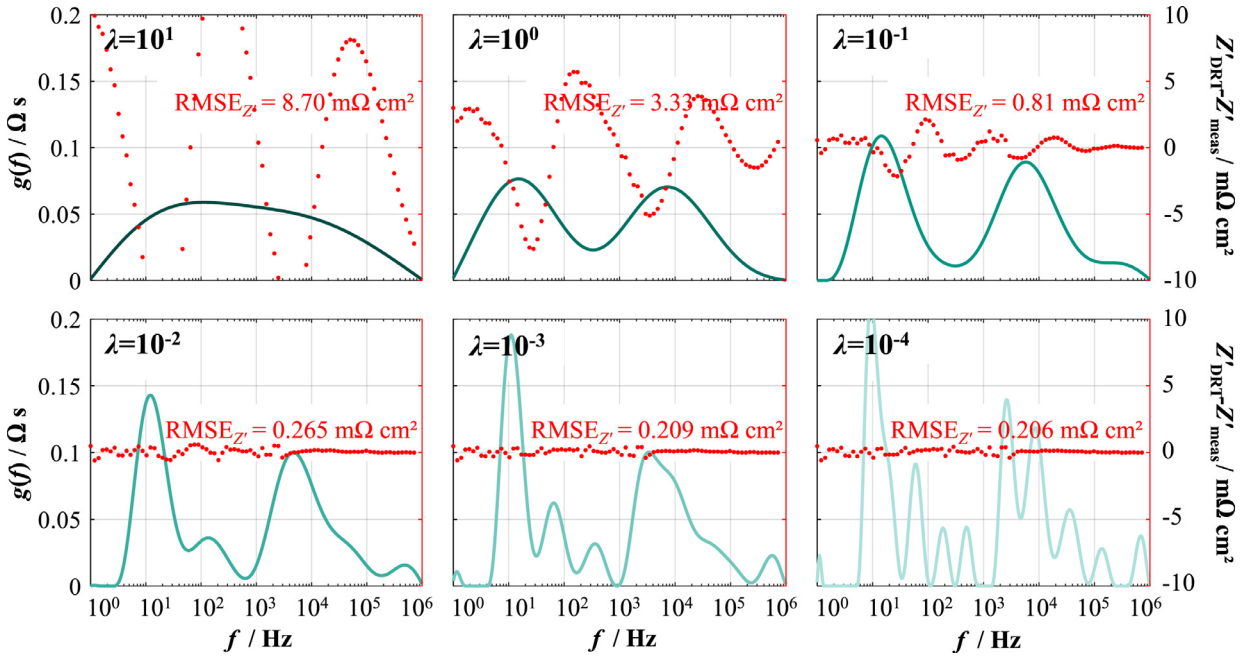

Fig. 7. Numerical DRTs of the measured impedance spectrum in Fig. 7 (a) calculated by the Tikhonov regularization with different λ-values. Also shown: the absolute error between the real part of the measured impedance (Z'_{meas}) and the real part calculated from the DRT spectrum (Z'_{DRT}). With decreasing λ the impact of the regularization diminishes, which results in a higher number of peaks in the DRT and thus a more accurate reproduction of the impedance. The measurement is recorded under OCV-conditions at 720 °C, with 20 % humidified hydrogen as fuel and ambient air as oxidant.

again emphasize that no universally valid lambda value exists. On the contrary, the optimal regularization strongly depends on (i) the investigated system, (ii) the measurement setup, and (iii) the test conditions. It must, therefore, be individually determined for each experiment.

4.2. Identification of electrochemical processes by DRT

This section introduces the usefulness of DRT to deconvolute impedance spectra of fuel cells. The first approach, a so-called black-box model, emulates the experimentally derived impedance spectra with a very general ECM (usually a series of RC-elements) and was first introduced in [62–64]. Because the RC-elements of the DRT can be easily transformed into the time domain, this approach can simulate the temporal current-voltage behavior of electrochemical devices [53]. While the evaluation of EIS by means of a general ECM as the DRT has the overriding advantage of not requiring *a priori* knowledge, it suffers from the flaw of missing physical interpretability. Therefore, this approach is preferably useful for control algorithms and dynamic system models.

In the second approach, the DRT is used to develop detailed physical models describing the experimentally derived impedance spectra as accurately as possible at all operating points of, i.e., a single cell made of SOFC or PEMFC components. Examples of such models are described below, they are applicable for assessing differently manufactured single cells or chemically and structurally modified electrodes, for quality assurance in fuel cell production, or durability investigations.

The total impedance of a PEMFC or SOFC is a sum of minor and major loss mechanisms, i.e., gas concentration and gas diffusion, oxygen reduction or hydrogen oxidation reaction, charge transfer reaction and charge transport, among others. While the impedance of model electrodes, especially point electrodes, depends on a single rate-determining step, understanding the impedance of technical electrodes is more complicated. Some impedance contributions, as described above, may be of equal quantity and their relaxation frequencies may overlap (to some extent). As a consequence, all of them have to be deconvoluted before a physically meaningful equivalent circuit model can be established.

The most common approach relies on using an *a priori* defined equivalent circuit model (ECM) from literature studies [7], whereon few impedance spectra are fitted by the Complex Nonlinear Least Squares (CNLS) algorithm. Our group does not recommend this approach, as it is not guaranteed, that all loss mechanisms in the sample under test are represented in the chosen ECM. ECMs with high complexity have many free parameters and can be easily fitted to all kinds of spectra, but the meaningfulness is ambiguous [47]. The DRT itself represents a simple but valid ECM [26] with approximately 100 RC-elements in series, but the corresponding 100 values of R and τ do not describe individual loss mechanisms.

Therefore, our group proposes to define a physically meaningful ECM by (i) a pre-identification of major, minor and/or overlapping loss mechanism via DRT, (ii) a sufficient number of impedance spectra of the sample under test sample at various operating conditions, and, thereafter, (iii) using permanently visible R and τ values as starting values for the CNLS-fit. Easy variable operating parameters for PEMFC and SOFC are cathode and anode gas compositions and fuel utilization, temperature, and current density.

In [30,56,65–67] we applied DRT-analysis and subsequent CNLS-fitting to electrodes and full cells. Impedance spectra were repeatedly measured after changing step-by-step one single operating parameter, i.e., hydrogen and steam partial pressures (pH_2, pH_2O) at the anode, or the oxygen partial pressure (pO_2) at the cathode or the cell temperature. Afterwards, the major and minor loss mechanisms were identified by deconvoluting all impedance spectra by the DRT, establishing a physically meaningful ECM, and evaluating all impedance spectra by CNLS-fits, using always the same (!) starting parameters. It should be pointed out, that meaningful operating parameter sets must be individually identified to restrict the number of measured impedance spectra. Assuming six spectra per variation - which in most cases provides sufficient resolution - the number of spectra to be measured would be 6^4 (= 1296).

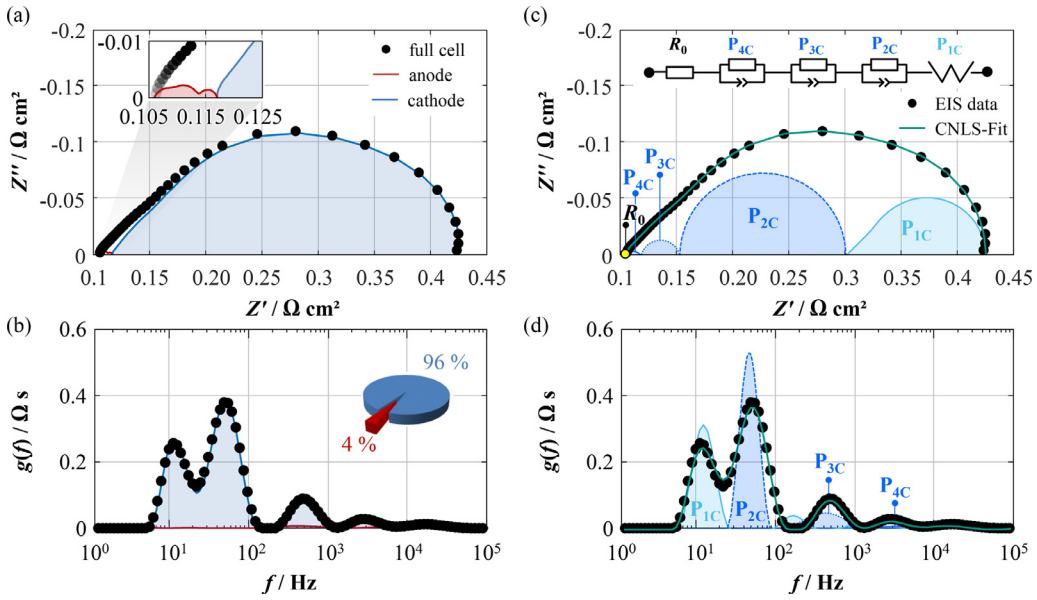

Fig. 8. (a) Measured impedance spectrum and (b) DRT of a PEMFC including the assignment of anode and cathode contribution to the overall cell polarization. The anode polarization is directly measured in symmetrical operation, while the cathode contribution is derived via subtraction from the full cell impedance. Figures (c) and (d) show a simulated impedance spectrum and the corresponding DRT based on a serial equivalent circuit model consisting of an ohmic resistance (R_0), a Warburg-element (P_{1C}) and three serial RQ-elements ($P_{2C\text{-}4C}$). The measurement was recorded at 382 mA cm^{-2}, 80 °C, with humidified hydrogen as fuel (70 % relative humidity) and humidified ambient air as oxidant (70 % relative humidity). Due to the predominant cathode polarization, the contributions of the anode processes are negligible under these operation conditions (EIS data from [57]).

In this sense, it is useful considering the physical nature of all contributing loss mechanisms. Gas diffusion in fuel cell electrodes is almost temperature-independent or increases only slightly with temperature [68], whereas charge transfer reactions are always thermally activated. In short, DRT peaks assignable to gas diffusion will stay almost of the same size, whereas DRT peaks of charge transfer reactions will decrease in size with increasing temperature. On the other hand, gas diffusion depends tremendously on the gas composition. The gas diffusion occurring in a (rather thick) SOFC anode substrate can be modeled by a GFLW (see Eq. (5), wherein the resistance, R_W, is related to [65,69]:

$$R_W = \left(\frac{RT}{2F}\right)^2 \cdot L_{An} \cdot \left(\frac{1}{D^{eff}_{H_2,An} \cdot pH_{2,An}} + \frac{1}{D^{eff}_{H_2O,An} \cdot pH_2O_{An}}\right). \quad (10)$$

Besides the well-known constants (R, F) and the parameters temperature, T, and the diffusion length, L_{An} (thickness of the anode substrate), R_W is defined by the effective (temperature dependent) diffusion coefficient:

$$D^{eff}_{i,An} = \frac{\varepsilon_{Pore,An}}{\tau_{Pore,An}} \cdot D_{mol,i,An}, \quad (11)$$

which depends on the porosity, ε, and the tortuosity, τ, of the substrate as well as the fuel composition (pH_2, pH_2O). Especially pure H_2 or H_2O (the latter is not advised, as the Ni grains will oxidize to NiO and expand by 30 % in volume), R_W will be seriously increased. Thus, a variation of the hydrogen to steam ratio is most appropriate for analyzing R_W. Additionally, the porosity to tortuosity relation is gained, as shown in [65] and [70], which is also required for other electrochemical [71] or multiphysical models [72,73].

The interested reader is referred to, i.e., for establishing physically meaningful, but still manageable ECMs for SOFCs in [48] and in [57,74,75] for PEMFCs. Most recently the DRT analysis has also found further uses in the growing research fields of other fuel cell types, such as the Molten Carbonate Fuel Cell (MCFC) [76] and the Protonic Ceramic Fuel Cell (PCFC) [77–79]. The found cell models are quite versatile and can be extended and used for different types of electrodes and cells, as shown in [80–84] for SOFC. In the following paragraphs, we present examples from our group for the two most thoroughly investigated fuel cells – a rather simple PEMFC model and models with increasing complexity for the SOFC.

PEMFC - DRT analysis on PEMFCs is still in the initial stages, and so far no established ECM exists that can consider all individual loss processes and their dependencies in a physically meaningful way [74,85–87]. By applying DRT analysis to PEMFC impedance spectra, the four major loss processes can be clearly resolved in the frequency range (see Fig. 8). Particular challenges for process identification and model development for PEMFCs are:

(i) the predominant cathode polarization,
(ii) the low operating temperature (promoting water formation in the pores),
(iii) the aqueous polymer membrane (allowing water transport along the membrane) and
(iv) the strong non-linearity close to OCV (requiring EIS under load).

The predominant cathode polarization can be solved by symmetrical operation of the PEMFC [57,75], which reveals that the anode contribution is negligible for a wide range of operation conditions (cf. Fig. 8 (a&b)). The other issues cause that almost every change of an operating parameter will influence the operating conditions (e.g. the relative humidity) at the electrodes and the electrolyte properties. Consequently, the interpretation of EIS data remains complex [88].

Based on a comprehensive parameter study, Heinzmann examined the essential dependencies of the individual loss processes and then designed the serial ECM shown in Fig. 8 (c&d). The model accounts for (i) the proton conduction of the polymer membrane, (ii) the gas diffusion of oxygen through the gas diffusion layer and the current collector of the cathode (including contact mesh and flowfield), (iii) the charge transfer kinetics at the cathode and (iv) the proton conduction in the ionomer of the cathode catalyst layer [57].

SOFC – The first ECM was established by our group as a series connection of one R, two RQs, one Gerischer- and one Warburg-element (see Table 1). Quite a number of operating parameter variations were necessary, i.e., temperature and gas composition (pH_2,

Table 1
List of the physical and electrochemical processes occurring in anode-supported SOFCs, together with their corresponding equivalent circuit model elements for the established serial model ECM [15] as well as the dependencies on the operating conditions.

	Physical Origin	Dependencies	Equivalent Circuits	
Cathode	gas diffusion in the cathode (including contact mesh and flowfield)	$pO_{2,Cat}$, T (low), j	RQ-element	P_{1C}
	oxygen surface exchange kinetics & bulk diffusion of O^{2-}	$pO_{2,Cat}$, T, j	Gerischer-element	P_{2C}
Electrolyte	oxygen ion transport in the electrolyte	T	resistor	R_0
Anode	gas diffusion in the anode substrate (including contact mesh and flowfield)	$pH_{2,An}$, pH_2O_{An}, T(low), j	GFLW-element	P_{1A}
	gas diffusion coupled with charge transfer reaction and ionic transport (AFL)	$pH_{2,An}$, pH_2O_{An},T, j	2 serial RQ-elements	P_{2A} P_{3A}

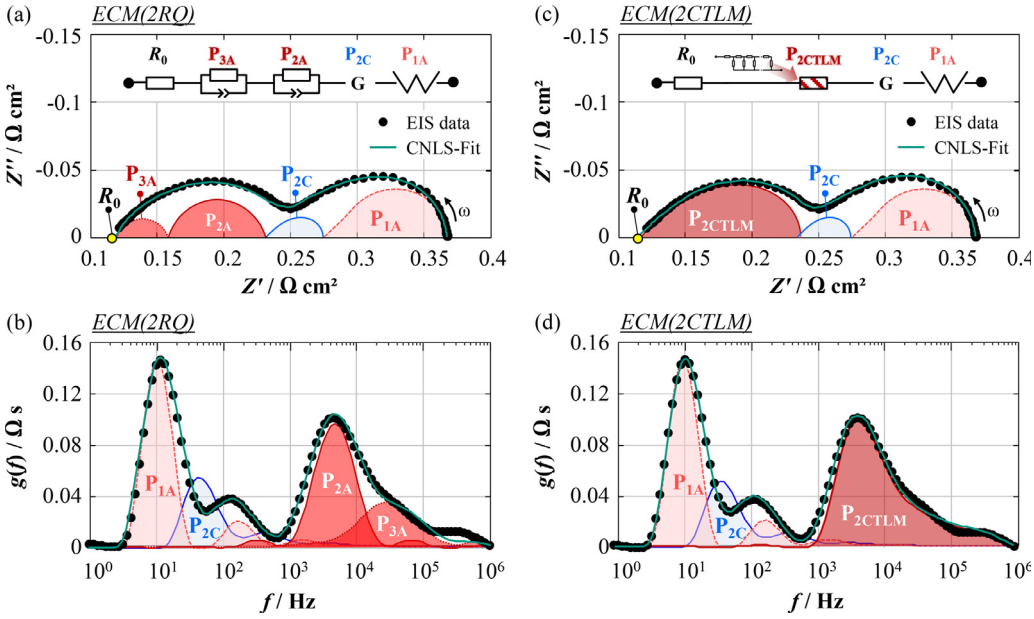

Fig. 9. Measured and simulated impedance spectra and DRTs of an anode supported SOFC based on different equivalent circuit models. Figures (a) and (b) are simulated with the established ECM with two RQ-elements - ECM(2RQ). In (c) and (d) the two RQ-elements are substituted by a physical parametrized TLM model - ECM(2CTLM). The cathode processes are blue and the anode processes are red. The measurement was recorded under OCV-conditions at 720 °C, with 20 % humidified hydrogen as fuel and ambient air as oxidant (EIS data from [56]).

pH_2O, pO_2,), resulting in approximately 100 impedance spectra - much lower than the 6^4 possible combinations. Fig. 9 (a) and (b) show the application of the model to the spectrum and the DRT of an anode-supported SOFC (ASC) with a mixed conducting cathode.

Despite the fact, that P_{1A} and P_{2C} strongly overlap, the CNLS-fitting delivers stable results because both processes are modelled by ECM elements with a meaningful description (i.e., Gerischer-element and Warburg-element). As mentioned above, the DRT was used in the CNLS-fit as an additional quality criterion. This is particularly valuable if the quantification of the EIS data is used for a parameterization of multiphysical models, as shown in [72] and [73].

4.3. Complex impedance models using DRT

The first extension of the above ECM was necessary for describing the additional loss mechanism linked to more complex fuels than pure hydrogen. In [66] Kromp analyzed a typical reformate mixture (pH_2 = 0.15 atm, pH_2O = 0.12 atm, pCO = 0.15 atm, pCO_2 = 0.13 atm, pN_2 = 0.45 atm) and discovered that only hydrogen is electrooxidized. Carbon monoxide as well as hydrocarbons are converted by catalytic processes on the Ni-surface. A new, additional loss process P_{ref} was added to the above ECM, arising at low frequencies because of the diffusion of rather large gas molecules. By adding 0.5 ppm H_2S to the fuel it could be shown that this low frequency process is related to a CO-conversion by the water-gas shift reaction (WGS) [89]. Fig. 10 demonstrates, that the total impedance increases while the low frequency process P_{ref} in the DRT decreases, as soon as sulfur poisoning takes place. Kromp explained this feature as a coupling of CO/CO_2-gas diffusion and the WGS on the nickel surfaces (which is diminished by adding H_2S to the fuel). The increase of the total impedance originates from larger contributions of P_{2A} and P_{3A} (H_2-electrooxidation in the AFL) and P_{1A} (H_2/H_2O-gas diffusion).

The second extension of Leonideś model was a replacement of the two RQ-elements (P_{2A} and P_{3A}) by a more accurate transmission line model (TLM, cf. Fig. 9 and Fig. 12) [56]. The two-channeled TLM (2CTLM) is best-suited to model the coupled (i) transport of oxygen ions in the solid oxide phase and (ii) the H_2-electrooxidation at the Ni phase (cf. Fig. 9 (c-d)). It has to be emphasized, that a TLM requires a set of essential parameters. It was indispensable to evaluate (i) microstructural parameters (i.e., the triple phase boundary length - l_{TPB}, the volume fraction and tortuosity of the 8YSZ-matrix – ε_{8YSZ} and τ_{8YSZ}) by FIB/SEM-tomography, (ii) the line specific resistance of the triple phase boundary (TPB) between Ni, YSZ and gas phase by EIS on patterned model anodes, (iii) the conductivity of the YSZ-matrix (usually altered by NiO interdiffusion during sintering [90] and, last but not least, (iv) using the DRT as an additional quality criterion in the CNLS-fit. It is important to state, that a measured impedance spectrum can always be fitted by a more simple ECM resulting in a lower error level. However, this would not necessarily provide a physically meaningful solution. In recent years, the applicability of TLM models to porous composite electrodes was also demonstrated by other research groups; e.g. Nielsen et al. for Ni/CGO infiltrated cermet anodes [91] and for LSM/YSZ cathodes [92], Shin et al. for LSM/YSZ cathodes and Ni/YSZ anodes [93,94], Mohammadi et al. for Ni/ScYSZ anodes [95].

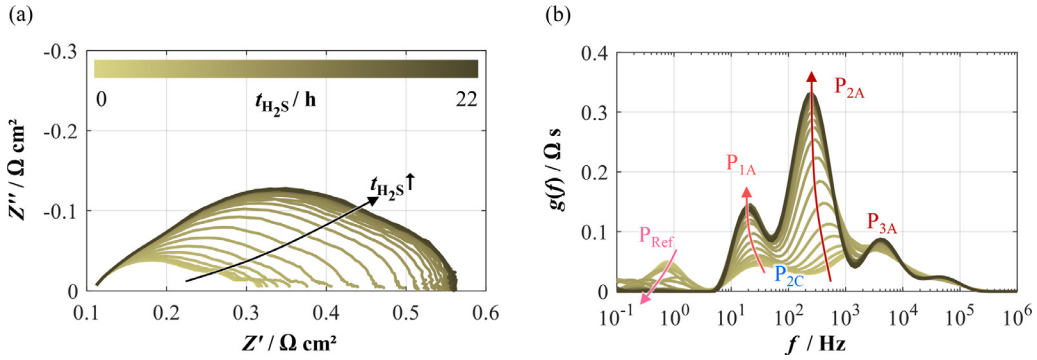

Fig. 10. Series of (a) EIS spectra and (b) DRTs during sulfur poisoning of an anode supported SOFC, operated with a reformate fuel ($x_{H_2S} = 0.5$ ppm) at 750 °C under OCV-conditions (EIS data from [89]).

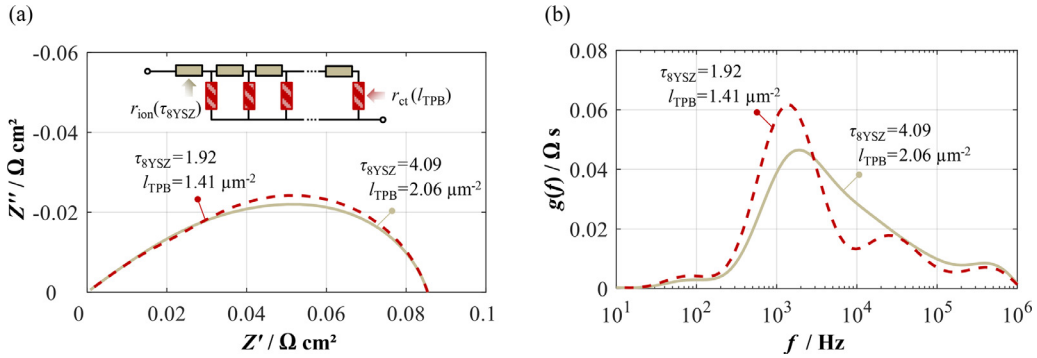

Fig. 11. Simulated (a) impedance spectra and (b) DRTs of different parameterized TLMs with a similar overall polarization resistance but different values of effective ionic conductivity (tortuosity - τ_{8YSZ}) and TPB-resistance (triple phase boundary length - l_{TPB}).

As a matter of fact, TLM fitting results are always ambiguous, as many parameters are required [56]. We emphasize to evaluate all required parameters by different experimental methods, to implement the DRT as an additional quality criterion (see above), or to control the agreement of DRTs from measured spectra and CNLS-fit. Fig. 11 illustrates this with two TLMs exhibiting a similar overall polarization resistance but different values of ionic conductivity and TPB-resistance. While only small differences are visible in the Nyquist plot, the DRT can clearly resolve the differences in the TLM. The origin of the similar impedance curves lies in the mathematical description of the TLM. Therein the loss contributions from the charge transfer reaction, r_{ct}, and the ion conduction, r_{ion}, are accounted as the quotient of both (r_{ct} / r_{ion}). Thus an enhancement of the charge transfer ($r_{ct}\downarrow \sim l_{TPB}\uparrow$) counteracts a weakening of the ion conduction ($r_{ion}\uparrow \sim \tau_{8YSZ}\uparrow$). This result demonstrates that the application of complex impedance models only provides reliable results in combination with a meaningful parameterization. Here the DRT shows up in particular as a powerful verification method.

However, a separate modelling approach for the (less than 5 to 20 µm thin) AFL and the (250 to 2000 µm thick) anode substrate is not always appropriate, as the electrochemical reactions can extend from the AFL into the anode substrate (depending on the design, i.e., the microstructure of both layers, operating conditions or degradation effects that change the original design). Therefore, in our latest publication on impedance modeling of SOFCs the 2CTLM was refined to reflect the impedance behavior of double-layered anodes, irrespective of which anode layer is electrochemically active [67]. For this purpose, the TLM structure was (i) extended by implementing the gas diffusion path - parametrized based on the microstructure of the gas kinetics - and (ii) linked for the number of anode layers. The efficient calculation of the impedance of this complex three-channeled TLM structure (3CTLM) is carried out numerically using a recently developed algorithm based on calculation methods from network analysis. With the new 3CTLM, the entire DRT (low frequency gas diffusion - $P_{1A;}$ and high frequency electrochemistry - P_{2A}&P_{3A}) of the fuel electrode can be simulated at once. Fig. 12 is a graphical compilation of all equivalent circuit models of anode-supported SOFCs developed by our group since 2008, and all of them originate from DRT as a tool for deconvoluting impedance spectra and/or using DRT as an additional quality criterion in the CNLS-fit.

The TLM modeling approach was recently transferred to PEMFC-electrodes in [60]. While TLM parametrization for SOFC anodes was based on independently evaluated microstructural and material parameters, the TLM parameters for PEMFC-electrodes are impacted by humidity. As humidity changes the ionic conductivity of the ionomer, this correlation can be used to identify the peaks in the DRT and to set up a meaningful TLM.

4.4. DRT analysis of degradation phenomena

Degradation phenomena in fuel cells always occur, among others, because of long operation times and/or not-intended system shut-downs. DRT is ideally suited to unroll individual degradation effects. Our group's investigation monitored continuously up to 1000 h operation time (Endler [51]) of state-of-the-art anode supported SOFCs. Applying Leonide's ECM (Fig. 12) to the large set of impedance data gave evidence, that the performance drop was essentially influenced by the mixed ionic–electronic conducting cathode. The cathodic part P_{2C}, initially by far the smallest, was superimposed by the much larger anodic gas diffusion P_{1A} with quite similar time constants (see Fig. 13(a)). But, as already introduced for Kromp's model, a change in fuel gas composition from H_2/H_2O to CO/CO_2 at the anode side shifted the anodic contribution to lower frequencies and thus, cleared the quantity of the cathode to the overall cell impedance (see Fig. 13(b)). The contri-

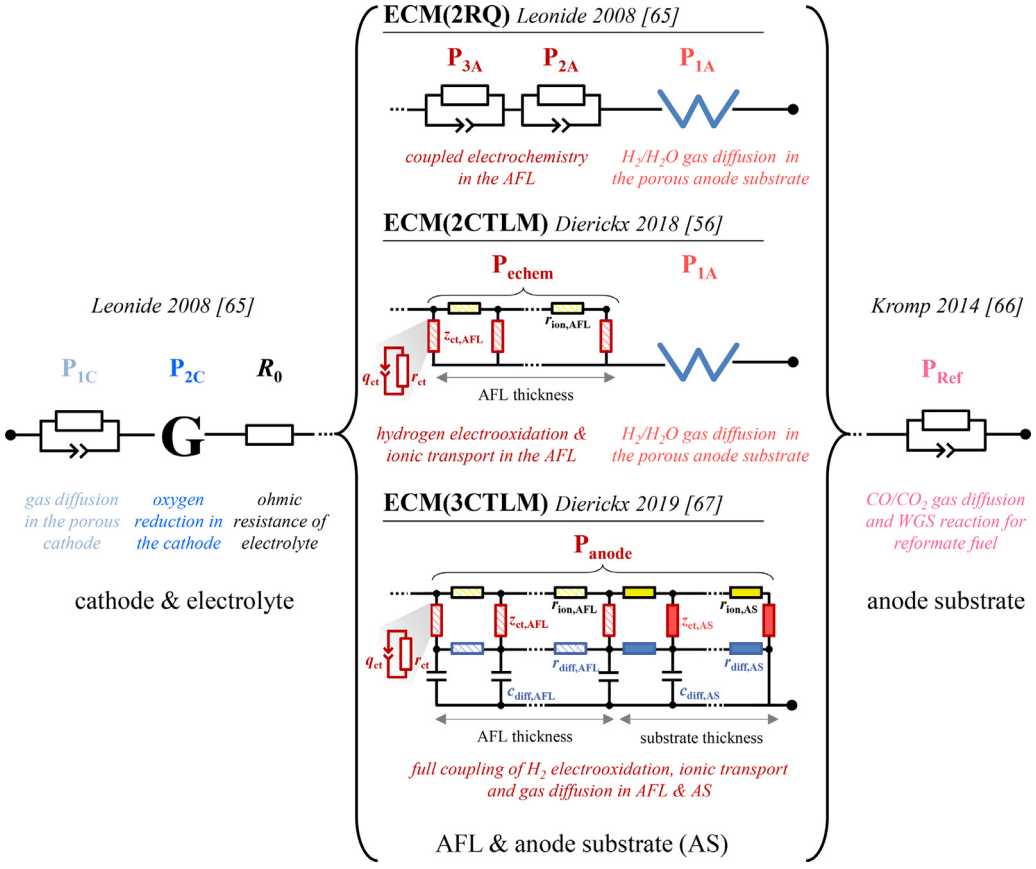

Fig. 12. Graphical compilation of all equivalent circuit models of anode-supported SOFCs developed and validated at the IAM-WET over the last 10 years. The depicted models (i) ECM(2RQ) [65], (ii) ECM(2CTLM) [56] and (iii) ECM(3CTLM) [67] differ with regard to the modelling of the anode double layer (anode functional layer – AFL; anode substrate – AS). In addition, the model extension for reformate operation (P_{ref}) is shown [66].

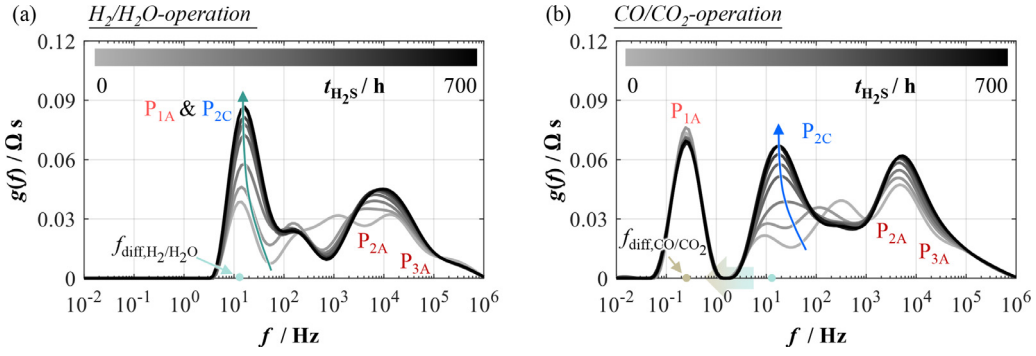

Fig. 13. DRTs of impedance spectra of an anode supported SOFC measured in (a) H_2/H_2O and (b) CO/CO_2 fuel during a durability test of 700 h in ambient air. Switching the fuel gas shifts the characteristic frequency (f_{diff}) of the diffusion due to the different molar masses of the gas components (EIS data from [50]).

bution of the Gerischer element, which stands for cathodic oxygen surface exchange kinetics & bulk diffusion of O^{2-}, increased by 310 %. At the same time, the sum of anodic contributions P_{1A}, P_{2A}, P_{3A} decreased from 92 % at the start to 73 % at 700 h. The DRT disclosed further, that the two RQ-elements P_{2A}&P_{3A} (charge-transfer reaction and ionic transfer in the AFL) decreased from initially 60 % of the total cell impedance to 50 % after 700 h, while the Warburg-element P_{1A} (gas diffusion in the AS) remained constant over the entire operation time.

Since then, the degradation phenomena analysis by DRT has been applied by our group in a number of studies. In example 2 in [96], DRT analyses the effect of chromium poisoning to SOFC performance, which is of importance when oxygen inflow at the cathode side interacts with metal bipolar plates or even metal piping in the SOFC stack. In example 3, DRT clears the effect of sulfur poisoning of Ni/YSZ cermet anodes [89], which occurs during reformate gas inflow, if H_2S impurity gas is not extracted carefully. In example 4 [82], the redox stability of strontium titanate based ASCs was proven superior to state-of-the-art Ni/YSZ anode functional layers, and in example 5 [97], first investigations on the interaction between biogas-based fuel and Ni/YSZ anodes are presented. DRT analysis disclosed, that the temperature-dependent difficulty of carbon deposition hinders first the hydrogen electrooxidation in the AFL (P_{2A}&P_{3A}) and second, after pore clogging, increases the gas diffusion polarization (P_{1A}) in the anode substrate. Comparable findings are reported by Subotić et. al. in [42] and Madi et. al. in [98]. Mogensens group analysed the kinetics of CO/CO_2 and H_2/H_2O reactions at Ni-based and ceria-based solid

oxide cell electrodes by EIS and DRT [99]. The performance change of a short stack operated in fuel cell and electrolysis modes was evaluated by EIS and DRT at the Research Center Jülich [100]. Sumi et.al. widened the application of EIS and DRT to the design of microtubular SOFCs [39,101]. All of these studies are stimulating the Distribution of Relaxation Times method as an indispensable tool not only for establishing accurate ECM models but also for deconvoluting aging phenomena in single cells and stacks.

5. Conclusion

This paper thoroughly explains the assessment of EIS measurements of polymer electrolyte and solid oxide fuel cells by DRT. For correct application, the fundamental mathematical characteristics of the DRT are presented, and both the analytical and the numerical DRT of common equivalent circuit elements are explained. We present indispensable insights into the impact of the EIS spectra quality and the Tikhonov regularization parameter lambda on the DRT. The Tikhonov regularization is used near universally because this method enables a reliable DRT calculation with limited error sources and good stability vs. noise in the measured EIS spectra. Identification of numerous physicochemical processes with close time constants in fuel cells is only attainable with a well-designed variation of operation parameters. Selected examples show the usefulness of DRT for establishing equivalent circuit models of differing complexity: a serial ECM for state-of-the-art planar SOFC and PEMFC, as well as the extension by 2-channel and 3-channel transmission line models mainly for SOFC.

In recent years other well-respected research groups have established their own EIS and DRT routines successfully. This work refers to a multitude of papers, which stimulate the Distribution of Relaxation Times method as an indispensable tool not only for establishing accurate ECM models, but also for deconvoluting aging phenomena in single cells of various chemistry and stacks of various design.

Declaration of Competing Interest

The authors declare that they have no known competing financial interests or personal relationships that could have appeared to influence the work reported in this paper.

Acknowledgements

The authors thank N. H. Menzler from Forschungszentrum Jülich and L. Jörissen from the Zentrum für Sonnenenergie- und Wasserstoffforschung for the generous supply of cells. We gratefully acknowledge funding from the Bundesministerium für Bildung und Forschung (BMBF 03SF0494F) and the Bundesministerium für Wirtschaft und Energie (BMWi 03ET6101B, 03ETB005E). Sincere thanks are given to J. Packham for proofreading the manuscript.

References

[1] F. Kohlrausch, W.A. Nippoldt, Ueber die Gültigkeit der Ohm'schen Gesetze für Elektrolyte und eine numerische Bestimmung des Leitungswiderstandes der verdünnten Schwefelsäure durch alternirende Ströme, Ann. Phys. 214 (1869) 280–298.
[2] F. Kohlrausch, Ueber electrische Widerstandsbestimmung mit Wechselströmen, Ann. Phys. 285 (1893) 225–256.
[3] O. Heaviside, Electrical Papers, Cambridge University Press, Cambridge, 2011.
[4] K.S. Cole, R.H. Cole, Dispersion and absorption in dielectrics I. Alternating current characteristics, J. Chem. Phys. 9 (1941) 341–351.
[5] J.E. Bauerle, Study of solid electrolyte polarization by a complex admittance method, J. Phys. Chem. Solids. 30 (1969) 2657–2670.
[6] J.R. Macdonald, J.A. Garber, Analysis of impedance and admittance data for solids and liquids, J. Electrochem. Soc. 124 (1977) 1022–1030.
[7] B.A. Boukamp, A nonlinear least squares fit procedure for analysis of immittance data of electrochemical systems, Solid State Ionics 20 (1986) 31–44.
[8] D.D. MacDonald, Reflections on the history of electrochemical impedance spectroscopy, Electrochim. Acta 51 (2006) 1376–1388.
[9] M.E. Orazem, B. Tribollet, Electrochemical Impedance Spectroscopy, John Wiley & Sons, Inc., Hoboken, NJ, USA, 2008.
[10] A. Lasia, Electrochemical Impedance Spectroscopy and its Applications, 1st ed., Springer, New York, New York, NY, 2014.
[11] D. Klotz, A. Weber, E. Ivers-Tiffée, Practical guidelines for reliable electrochemical characterization of solid oxide fuel cells, Electrochim 227 (2017) 110–126.
[12] B.A. Boukamp, A linear Kronig-Kramers transform test for immittance data validation, J. Electrochem. Soc. 142 (1995) 1885.
[13] M. Schönleber, D. Klotz, E. Ivers-Tiffée, A method for improving the robustness of linear Kramers-Kronig validity tests, Electrochim. Acta 131 (2014) 20–27.
[14] http://www.iam.kit.edu/wet/english/Lin-KK.php, (2015).
[15] E. Schweidler, Studien über die Anomalien im Verhalten der Dielektrika, Ann. Phys. 328 (1907) 711–770.
[16] K.W. Wagner, Zur Theorie der unvollkommenen Dielektrika, Ann. Phys. 345 (1913) 817–855.
[17] M. Fuoss, J.G. Kirkwood, Electrical properties of solids. VIII. Dipole moments in polyvinyl chloride-Diphenil systems - dipole moments distributions, J Am Chem Soc 63 (1941) 385–394.
[18] D.L. Misell, R.J. Sheppard, The application of deconvolution techniques to dielectric data, 1973.
[19] K. Giese, On the numerical evaluation of the dielectric relaxation time distribution function from permittivity data, Adv. Mol. Relax. Process. 5 (1973) 363–373.
[20] P. Colonomos, R.G. Gordon, Bounded error analysis of experimental distributions of relaxation times, J. Chem. Phys. 71 (1979) 1159–1166.
[21] J.L. Salefran, Y. Dutuit, The use of a discriminative window in deconvolution method applied to dielectric data, J. Chem. Phys. 74 (1981) 3056–3063.
[22] A.D. Franklin, H.J. De Bruin, The fourier analysis of impedance spectra for electroded solid electrolytes, Phys. Status Solidi. 75 (1983) 647–656.
[23] F.D. Morgan, D.P. Lesmes, Inversion for dielectric relaxation spectra, J, Chem. Phys. 100 (1994) 671–681.
[24] K.S. Paulson, S. Jouravleva, C.N. McLeod, Dielectric relaxation time spectroscopy, IEEE Trans. Biomed. Eng. 47 (2000) 1510–1517.
[25] H. Schichlein, A.C. Müller, M. Voigts, A. Krügel, E. Ivers-Tiffée, Deconvolution of electrochemical impedance spectra for the identification of electrode reaction mechanisms in solid oxide fuel cells, J. Appl. Electrochem. 32 (2002) 875–882.
[26] M. Schönleber, E. Ivers-Tiffée, Approximability of impedance spectra by RC elements and implications for impedance analysis, Electrochem. Commun 58 (2015) 15–19.
[27] A. Schiefer, M. Heinzmann, A. Weber, Inductive Low-Frequency Processes in PEMFC-Impedance Spectra, Fuel Cells (2020) 1–8.
[28] C. Groetsch, The theory of tikhonov regularization for fredholm equations of the first kind, Pitman Publishing, Boston, 1984.
[29] A.N. Tikhonov, A.V. Goncharsky, V.V. Stepanov, A.G. Yagola, Numerical Methods for the Solution of Ill-Posed Problems, Springer Netherlands, Dordrecht, 1995.
[30] V. Sonn, A. Leonide, E. Ivers-Tiffée, Combined Deconvolution and CNLS Fitting Approach Applied on the Impedance Response of Technical Ni/8YSZ Cermet Electrodes, J. Electrochem. Soc. 155 (2008) B675.
[31] http://cpc.cs.qub.ac.uk/summaries/ACGH_v1_0.html, (1992).
[32] J. Weese, A reliable and fast method for the solution of Fredhol integral equations of the first kind based on Tikhonov regularization, Comput. Phys. Commun. 69 (1992) 99–111.
[33] T.H. Wan, M. Saccoccio, C. Chen, F. Ciucci, Influence of the discretization methods on the distribution of relaxation times deconvolution: implementing radial basis functions with DRTtools, Electrochim. Acta. 184 (2015) 483–499.
[34] https://sites.google.com/site/drttools/, (2015).
[35] B.A. Boukamp, A. Rolle, Use of a distribution function of relaxation times (DFRT) in impedance analysis of SOFC electrodes, Solid State Ionics 314 (2018) 103–111.
[36] B.A. Boukamp, Fourier transform distribution function of relaxation times; application and limitations, Electrochim. Acta. 154 (2015) 35–46.
[37] C. Graves, S.D. Ebbesen, M. Mogensen, Co-electrolysis of CO2 and H2O in solid oxide cells: Performance and durability, Solid State Ionics 192 (2011) 398–403.
[38] Z. Wuillemin, Y. Antonetti, C. Beetschen, O. Millioud, S. Ceschini, H. Madi, J. Van Herle, Local activation and degradation of electrochemical processes in a SOFC, ECS Trans 57 (2013) 561–570.
[39] H. Sumi, T. Yamaguchi, K. Hamamoto, T. Suzuki, Y. Fujishiro, Electrochemical analysis for anode-supported microtubular solid oxide fuel cells in partial reducing and oxidizing conditions, Solid State Ionics 262 (2014) 407–410.
[40] F. Ciucci, C. Chen, Analysis of electrochemical impedance spectroscopy data using the distribution of relaxation times: A Bayesian and hierarchical Bayesian approach, Electrochim 167 (2015) 439–454.
[41] Y. Zhang, Y. Chen, M. Li, M. Yan, M. Ni, C. Xia, A high-precision approach to reconstruct distribution of relaxation times from electrochemical impedance spectroscopy, J, Power Sources 308 (2016) 1–6.
[42] V. Subotić, C. Schluckner, J. Strasser, V. Lawlor, J. Mathe, J. Rechberger, H. Schroettner, C. Hochenauer, In-situ electrochemical characterization methods for industrial-sized planar solid oxide fuel cells Part I: Methodology, qualification and detection of carbon deposition, Electrochim 207 (2016) 224–236.

[43] A. Nechache, A. Mansuy, M. Petitjean, J. Mougin, F. Mauvy, B.A. Boukamp, M. Cassir, A. Ringuedé, Diagnosis of a cathode-supported solid oxide electrolysis cell by electrochemical impedance spectroscopy, Electrochim 210 (2016) 596–605.

[44] K. Kobayashi, Y. Sakka, T.S. Suzuki, Development of an electrochemical impedance analysis program based on the expanded measurement model, J. Ceram. Soc. Japan. 124 (2016) 943–949.

[45] S. Katayama, H. Nakai, A. Kita, Electrochemical impedance analysis of LiCoO2/Graphite lithium ion batteries by distribution of relaxation times method, Meet. Abstr. 2016-02 (2016) 324.

[46] E. Ivers-Tiffée, A. Weber, Evaluation of electrochemical impedance spectra by the distribution of relaxation times, J. Ceram. Soc. Jpn. 125 (2017) 193–201.

[47] J.R. Macdonald, E. Barsoukov, Impedance Spectroscopy, 2nd ed., John Wiley \&; Sons, Inc., Hoboken, NJ, USA, 2005.

[48] A. Leonide, SOFC modeling and parameter identification by means of impedance spectroscopy, Universität Karlsruhe (TH) (2010).

[49] B.A. Boukamp, Derivation of a Distribution Function of Relaxation Times for the (fractal) Finite Length Warburg, Electrochim. Acta. 252 (2017) 154–163.

[50] F. Dion, A. Lasia, The use of regularization methods in the deconvolution of underlying distributions in electrochemical processes, J. Electroanal. Chem. 475 (1999) 28–37.

[51] C. Endler, A. Leonide, A. Weber, F. Tietz, E. Ivers-Tiffée, Time-dependent electrode performance changes in intermediate temperature solid oxide fuel cells, J. Electrochem. Soc. 157 (2010) B292.

[52] B.A. Boukamp, A. Rolle, Analysis and application of distribution of relaxation times in solid state ionics, Solid State Ionics 302 (2017) 12–18.

[53] J.P. Schmidt, P. Berg, M. Schönleber, A. Weber, E. Ivers-Tiffée, The distribution of relaxation times as basis for generalized time-domain models for Li-ion batteries, J. Power Sources 221 (2013) 70–77.

[54] H.W. Engl, M. Hanke, A. Neubauer, Regularization of Inverse Problems, Springer, Netherlands, 2000.

[55] B.A. Boukamp, Practical application of the Kramers-Kronig transformation on impedance measurements in solid state electrochemistry, Solid State Ionics 62 (1993) 131–141.

[56] S. Dierickx, J. Joos, A. Weber, E. Ivers-Tiffée, Advanced impedance modelling of Ni/8YSZ cermet anodes, Electrochim. Acta. 265 (2018) 736–750.

[57] M. Heinzmann, A. Weber, E. Ivers-Tiffée, Advanced impedance study of polymer electrolyte membrane single cells by means of distribution of relaxation times, J. Power Sources 402 (2018) 24–33.

[58] M. Saccoccio, T.H. Wan, C. Chen, F. Ciucci, Optimal regularization in distribution of relaxation times applied to electrochemical impedance spectroscopy: Ridge and Lasso regression methods - a theoretical and experimental Study, Electrochim. Acta. 147 (2014) 470–482.

[59] J.P. Tomba, M.D.L.P. Miguel, C.J. Perez, Correction of optical distortions in dry depth profiling with confocal Raman microspectroscopy, J. Raman Spectrosc. 42 (2011) 1330–1334.

[60] T. Correia, A. Gibson, M. Schweiger, J. Hebden, Selection of regularization parameter for optical topography, J. Biomed. Opt. 14 (2009) 034044.

[61] M.B. Choi, J. Shin, H. Il Ji, H. Kim, J.W. Son, J.H. Lee, B.K. Kim, H.W. Lee, K.J. Yoon, Interpretation of impedance spectra of solid oxide fuel cells: L-Curve criterion for determination of regularization parameter in distribution function of relaxation times technique, Jom 71 (2019) 3825–3834.

[62] P. Agarwal, Measurement models for electrochemical impedance spectroscopy, J. Electrochem. Soc. 139 (1992) 1917.

[63] P. Agarwal, M.E. Orazem, Application of measurement models to impedance spectroscopy II. Determination of the stochastic contribution to the error structure, J. Electrochem. Soc. 142 (1995) 4149–4158.

[64] P. Agarwal, Application of measurement models to impedance spectroscopy IL evaluation of consistency with the kramers-kronig relations, J. Electrochem. Soc. 142 (1995) 4159–4168.

[65] A. Leonide, V. Sonn, A. Weber, E. Ivers-Tiffée, Evaluation and modeling of the cell resistance in anode-supported solid oxide fuel cells, J. Electrochem. Soc. 155 (2008) B36.

[66] A. Kromp, A. Leonide, A. Weber, E. Ivers-Tiffée, Electrochemical analysis of reformate-fuelled anode supported SOFC, J. Electrochem. Soc. 158 (2011) B980.

[67] S. Dierickx, T. Mundloch, A. Weber, E. Ivers-Tiffée, Advanced impedance model for double-layered solid oxide fuel cell cermet anodes, J. Power Sources 415 (2019) 69–82.

[68] J. Hayd, E. Ivers-Tiffée, Detailed electrochemical study on nanoscaled La0.6Sr 0.4CoO3-δ SOFC thin-film cathodes in dry, humid and CO2-containing atmospheres, J. Electrochem. Soc. (2013) 160.

[69] S. Primdahl, Gas diffusion impedance in characterization of solid oxide fuel cell anodes, J. Electrochem. Soc. 146 (1999) 2827.

[70] Y. Zhang, Y. Chen, F. Chena, In-situ quantification of solid oxide fuel cell electrode microstructure by electrochemical impedance spectroscopy, J. Power Sources 277 (2015) 277–285.

[71] A. Leonide, S. Hansmann, A. Weber, E. Ivers-Tiffée, Performance simulation of current/voltage-characteristics for SOFC single cell by means of detailed impedance analysis, J. Power Sources 196 (2011) 7343–7346.

[72] A. Bertei, E. Ruiz-Trejo, F. Tariq, V. Yufit, A. Atkinson, N.P. Brandon, Validation of a physically-based solid oxide fuel cell anode model combining 3D tomography and impedance spectroscopy, Int. J. Hydrogen Energy. 41 (2016) 22381–22393.

[73] N. Russner, S. Dierickx, A. Weber, R. Reimert, E. Ivers-Tiffée, Multiphysical modelling of planar Solid oxide fuel cell stack layers, J. Power Sources. (2019).

[74] M. Heinzmann, A. Weber, E. Ivers-Tiffée, Impedance modelling of porous electrode structures in polymer electrolyte membrane fuel cells, J. Power Sources. (2019) 444.

[75] A. Weiß, S. Schindler, S. Galbiati, M.A. Danzer, R. Zeis, Distribution of relaxation times analysis of high-temperature PEM fuel cell impedance spectra, Electrochim. Acta. 230 (2017) 391–398.

[76] F. Santoni, M. Della Pietra, D. Pumiglia, C. Boigues Muñoz, S.J. McPhail, V. Cigolotti, S.W. Nam, M.G. Kang, S.P. Yoon, Accurate in-operando study of molten carbonate fuel cell degradation processes -part I: Physiochemical processes individuation, Electrochim 291 (2018) 343–352.

[77] N. Shi, F. Su, D. Huan, Y. Xie, J. Lin, W. Tan, R. Peng, C. Xia, C. Chen, Y. Lu, Performance and DRT analysis of P-SOFCs fabricated using new phase inversion combined tape casting technology, J. Mater. Chem. A. 5 (2017) 19664–19671.

[78] X. Wang, Z. Ma, T. Zhang, J. Kang, X. Ou, P. Feng, S. Wang, F. Zhou, Y. Ling, Charge-transfer modeling and polarization drt analysis of proton ceramics fuel cells based on mixed conductive electrolyte with the modified anode–electrolyte interface, ACS Appl. Mater. Interfaces. 10 (2018) 35047–35059.

[79] Y. Wu, K. Li, Y. Yang, W. Song, Z. Ma, H. Chen, X. Ou, L. Zhao, M. Khan, Y. Ling, Investigation of Fe-substituted in BaZr0.8Y0.2O3-δ proton conducting oxides as cathode materials for protonic ceramics fuel cells, J. Alloys Compd 814 (2020) 152220.

[80] A. Leonide, B. Rüger, A. Weber, W.A. Meulenberg, E. Ivers-Tiffé, Impedance study of alternative (La,Sr) FeO3-δ and (La,Sr) (Co,Fe) O3-δ MIEC Cathode Compositions, J. Electrochem. Soc. (2010) 157.

[81] P. Blennow, J. Hjelm, T. Klemensø, S. Ramousse, A. Kromp, A. Leonide, A. Weber, Manufacturing and characterization of metal-supported solid oxide fuel cells, J. Power Sources 196 (2011) 7117–7125.

[82] Q. Ma, F. Tietz, A. Leonide, E. Ivers-Tiffée, Electrochemical performances of solid oxide fuel cells based on Y-substituted SrTiO3 ceramic anode materials, J. Power Sources 196 (2011) 7308–7312.

[83] F. Han, R. Mücke, T. Van Gestel, A. Leonide, N.H. Menzler, H.P. Buchkremer, D. Stöver, Novel high-performance solid oxide fuel cells with bulk ionic conductance dominated thin-film electrolytes, J. Power Sources 218 (2012) 157–162.

[84] T. Ramos, M. Søgaard, M.B. Mogensen, Electrochemical Characterization of Ni/ScYSZ Electrodes as SOFC Anodes, J. Electrochem. Soc. 161 (2014) F434–F444.

[85] Z. Xie, S. Holdcroft, Polarization-dependent mass transport parameters for orr in perfluorosulfonic acid ionomer membranes: An EIS study using microelectrodes, J. Electroanal. Chem. 568 (2004) 247–260.

[86] N. Fouquet, C. Doulet, C. Nouillant, G. Dauphin-Tanguy, B. Ould-Bouamama, Model based PEM fuel cell state-of-health monitoring via ac impedance measurements, J. Power Sources. 159 (2006) 905–913.

[87] N. Wagner, K.A. Friedrich, Application of electrochemical impedance spectroscopy for fuel cell characterization: PEFC and oxygen reduction reaction in alkaline solution, Fuel Cells 9 (2009) 237–246.

[88] X. Yuan, H. Wang, J. Colin Sun, J. Zhang, AC impedance technique in PEM fuel cell diagnosis-A review, Int. J. Hydrogen Energy 32 (2007) 4365–4380.

[89] A. Kromp, S. Dierickx, A. Leonide, A. Weber, E. Ivers-Tiffée, Electrochemical analysis of sulfur-poisoning in anode supported SOFCs fuelled with a model reformate, J. Electrochem. Soc. 159 (2012) B597–B601.

[90] T. Shimonosono, H. Kishimoto, M.E. Brito, K. Yamaji, T. Horita, H. Yokokawa, Phase transformation related electrical conductivity degradation of NiO doped YSZ, Solid State Ionics 225 (2012) 69–72.

[91] J. Nielsen, T. Klemensø, P. Blennow, Detailed impedance characterization of a well performing and durable Ni:CGO infiltrated cermet anode for metal-supported solid oxide fuel cells, J. Power Sources 219 (2012) 305–316.

[92] J. Nielsen, J. Hjelm, Impedance of SOFC electrodes: A review and a comprehensive case study on the impedance of LSM:YSZ cathodes, Electrochim. Acta. 115 (2014) 31–45.

[93] E.C. Shin, P.A. Ahn, H.H. Seo, D.T. Nguyen, S.D. Kim, S.K. Woo, J.H. Yu, J.S. Lee, Pinning-down polarization losses and electrode kinetics in cermet-supported LSM solid oxide cells in reversible operation, Solid State Ionics 277 (2015) 1–10.

[94] E.C. Shin, J. Ma, P.A. Ahn, H.H. Seo, D.T. Nguyen, J.S. Lee, Deconvolution of Four Transmission-Line-Model Impedances in Ni-YSZ/YSZ/LSM Solid Oxide Cells and Mechanistic Insights, Electrochim. Acta 188 (2016) 240–253.

[95] R. Mohammadi, M. Søgaard, T. Ramos, M. Ghassemi, M. Mogensen, Electrochemical impedance modeling of a solid oxide fuel cell anode, Fuel Cells 14 (2014) 645–659.

[96] M. Kornely, A. Neumann, N.H. Menzler, A. Leonide, A. Weber, E. Ivers-Tiffée, Degradation of anode supported cell (ASC) performance by Cr-poisoning, J. Power Sources 196 (2011) 7203–7208.

[97] A. Leonide, A. Weber, E. Ivers-Tiffée, Electrochemical analysis of biogas fueled anode supported SOFC, ECS Trans 35 (2011) 2961–2968.

[98] H. Madi, A. Lanzini, D. Papurello, S. Diethelm, C. Ludwig, M. Santarelli, J. Van herle, Solid oxide fuel cell anode degradation by the effect of hydrogen chloride in stack and single cell environments, J. Power Sources 326 (2016) 349–356.

[99] C. Graves, C. Chatzichristodoulou, M.B. Mogensen, Kinetics of CO/CO2 and H2/H2O reactions at Ni-based and ceria-based solid-oxide-cell electrodes, Faraday Discuss. 182 (2015) 75–95.

[100] Q. Fang, L. Blum, N.H. Menzler, Performance and degradation of solid oxide electrolysis cells in stack, J. Electrochem. Soc. 162 (2015) F907–F912.

[101] H. Sumi, H. Shimada, Y. Yamaguchi, T. Yamaguchi, Y. Fujishiro, Degradation evaluation by distribution of relaxation times analysis for microtubular solid oxide fuel cells, Electrochim. Acta. 339 (2020) 135913.